FULL PAPER

Toward Full Exposure of 'Active Sites': Nanocarbon Electrocatalyst with Surface Enriched Nitrogen for Superior Oxygen Reduction and Evolution Reactivity

Gui-Li Tian, Qiang Zhang,* Bingsen Zhang, Yu-Guang Jin, Jia-Qi Huang, Dang Sheng Su,* and Fei Wei*

The oxygen reduction reaction (ORR) and oxygen evolution reaction (OER) play a decisive role for the efficiency of fuel cells and metal-air batteries. The nitrogen doped carbon materials with low cost and long durability are potential catalysts to replace precious metal catalyst for oxygen electrochemistry; however, the unexposed active sites induced by the bulk dopant atoms are hardly accessible and consequently scarcely contribute to the catalytic property. In this study, carbon nanotubes (CNTs) are selected as the platform to demonstrate the potential of full exposure of 'active sites' at the surface. Novel N-doped carbon coaxial nanocables with the pristine CNTs as the core and the N-doped carbon layers as the shell are proposed. The accessible and efficient utilization of the integrated nitrogen atoms enriched on the surface, together with the undestroyed intact inner walls, render the electrocatalyst much enhanced electrocatalytic activity and high electrical conductivity of 3.3 S cm^{-1}, therefore, N-doped nanocables afford higher oxygen reduction current, ~51 mV positively shift onset potential, low peroxide generation, as well as lower overpotential and higher current for oxygen evolution reaction.

1. Introduction

The oxygen electrochemistry involved energy systems, such as fuel cells and metal-air batteries, are of great attractive prospect due to their high capacity and environmental friendliness.[1,2] As the main cathodic and anodic reaction, respectively, the oxygen reduction reaction (ORR) and oxygen evolution reaction (OER) play a decisive role for the efficiency of such energy conversion and storage devices. However, both of the ORR and OER are kinetically sluggish due to the complicated multi-electron transfer process. The catalysts based on precious metals like

Pt, Ir, and Ru, et al. are usually effective to boost the ORR or OER rate,[2,3] but their practical applications are severely limited by the prohibitive cost, scarce resource, and poor durability. Therefore, non-noble metal material and even non-metal material were explored for overcoming the limitation of the precious metal electrocatalysts for ORR and OER.[4–6] In particular, the bifunctional electrocatalysts for both OER and ORR reactions were highly desired for the unitized regenerative fuel cells (URECs), which can do the water electrolysis in regenerative mode and function in the other mode as a fuel cell recombining oxygen and hydrogen gas to produce electricity. Recently, Dai and co-workers[6] reported that the nitrogen-doped carbon nanotubes (NCNTs) acted as an excellent electrocatalyst candidate with better electrocatalytic activity, long-term stability, and tolerance to crossover effect than the conventional Pt for ORR. Furthermore, the nitrogen-doped carbon materials were found as the efficient oxygen evolution electrocatalysts with comparable activity to those of iridium and cobalt oxide catalysts.[5] The N-doped carbon materials were with low cost, high catalytic activity, long durability, as well as abundant resource on earth, which were potential catalysts for oxygen electrochemistry and highly concerned recently.[5,7]

The incorporation of nitrogen atoms into the carbon frameworks can effectively modulate the electronic structure of the surrounding carbon atoms and tune the local charge density distribution,[8] which results in the improvement of the chemical reactivity and subsequently promotes the catalytic performance.[9] In heterogeneous catalysis, the active sites of the catalysts are expected to be exposed at the surface which can be accessible to the reactants as much as possible in order to achieve high catalytic efficiency. However, for most of routine NCNTs directly synthesized by chemical vapor deposition (CVD) growth and chemical doping,[6,10,11] the incorporated N atoms distributed uniformly in general, whereas the active sites induced by the dopant atoms in the inner walls of NCNTs were hardly accessible and consequently contributed to the catalytic property scarcely. Besides, the bamboo-like structure or the cup-stacked structure of the routine NCNTs render complex packing of graphene layers, which hinder the rapid electron

G.-L. Tian, Prof. Q. Zhang, Dr. Y.-G. Jin,
Dr. J.-Q. Huang, Prof. F. Wei
Beijing Key Laboratory of Green Chemical Reaction
Engineering and Technology
Department of Chemical Engineering
Tsinghua University
Beijing 100084, PR China
E-mail: zhang-qiang@mails.tsinghua.edu.cn; wf-dce@tsinghua.edu.cn
Prof. B. S. Zhang, Prof. D. S. Su
Institute of Metal Research
Chinese Academy of Sciences
Shenyang 110016, PR China
E-mail: dangsheng@fhi-berlin.mpg.de

**ADVANCED
FUNCTIONAL
MATERIALS**

www.afm-journal.de

*Materials
Views*

www.MaterialsViews.com

FULL PAPER

transport along the graphene layers. In this regard, it's highly desired for an efficient NCNT electrocatalyst to selectively incorporate the N atoms into the carbon nanotubes (CNTs) on the surface to fully expose the active sites while the inner continuous CNT walls are well preserved.

In this contribution, a nanocarbon electrocatalyst with surface enriched nitrogen was proposed to fully expose 'active sites' at the surface for superior oxygen reduction and evolution reactivity. The nitrogen-doped coaxial carbon nanocables, denoted as CNT@NCNT, with the pristine CNTs as the core and the N-doped carbon layers as the shell were selected as the model system (**Figure 1**). The active sites rendered by the surface enriched dopant atoms were expected to be more accessible and effective to catalyze the oxygen involved electrochemical reactions. Therefore, the as-obtained CNT@NCNT nanocables afforded higher ORR/OER current compared with the routine bulk doped NCNTs.

2. Results and Discussion

2.1. Structure of Nanocarbon Electrocatalyst with Surface Enriched Nitrogen

The microstructures of CNT@NCNT electrocatalyst with surface enriched nitrogen were presented in **Figure 2**. Both pristine CNTs and NCNTs mass produced in a fluidized bed reactor[12] were selected as control samples. The CNT@NCNT coaxial nanocables fabricated by CVD of nitrogen-containing compounds on the pristine CNTs were similar with that of the pristine CNTs (Figure S1). The N-doped turbostratic carbon layers were epitaxial grown on the outer walls of pristine CNTs, resulting in the CNT@NCNT coaxial nanocables constituted by the cylindrical CNT walls and the wrinkled N-doped layers (Figure 2c). The higher D/G ratio in Raman spectra (Figure S2) implied the high-density defects of CNT@NCNT due to the incorporation of N atoms. With prolonging the epitaxial growth, the N-doped layers became thicker. Consequently, the CNT@NCNT nanocables were with a larger outer diameter (Figure S3). The number of N-doped turbostratic carbon layers can be modulated from almost one to several dozens, corresponding to the
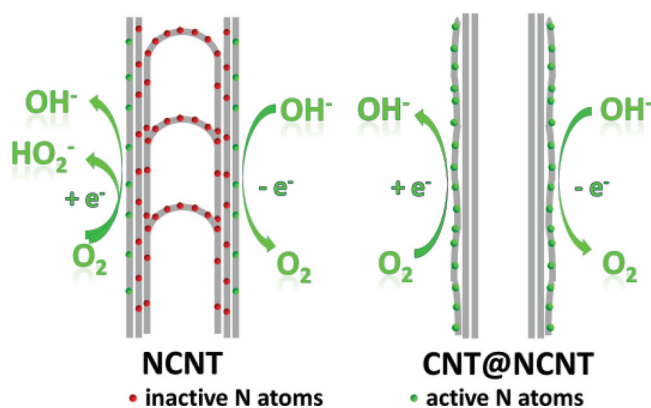
surface N/C ratios from 0.0238 to 0.145 (**Table 1** and S1) by controlling epitaxial growth duration from 0.5 to 3 h, respectively. The CNT@NCNT products were denoted as CNT@NCNT, CNT@NCNT-1, CNT@NCNT-3 corresponding to the epitaxial growth duration of 0.5, 1, and 3 h, respectively.

In order to confirm the doping of N atoms in the CNT@NCNT nanocables, energy filtered transmission electron microscopy (EFTEM) was employed to clarify the distribution of N atoms. The N atoms were indeed concentrated on the surface of the nanocable (Figure 2d & 2e), which is quite different from the homogeneous distribution of N atoms in bulk doped NCNTs.[11,13] The electron energy loss spectrum (EELS) in Figure 2f and S4a also confirm the contribution of nitrogen in the as obtained nanocable. Most carbon atoms were sp^2-hybridized as reflected by the characteristic π^* and σ^* transitions in the carbon K edge.[14] The surface nitrogen amount was further determined by X-ray photoelectron spectroscopy (XPS) analysis (Figure 2g, S4b, and S5). The N 1s spectrum was deconvoluted into five peaks which were assigned to pyridinic N (398.4 eV), pyrrolic N (399.5 eV), quaternary N (401.0 eV), oxidized N (402.7 eV), and chemsorbed N (404.9 eV), respectively (Figure 2g). The relative ratios of the N-containing functional groups were summarized in Table S2. Furthermore, elemental analysis *via* combustion was carried out to determine the total bulk content of nitrogen element in the electrocatalysts. Notably, the atomic N/C ratio determined by XPS (0.0238) was higher than that determined by elemental analysis (0.0219) for the CNT@NCNT nanocables, indicating that the N atoms were concentrated on the surface of the CNT@NCNT nanocables. In contrast, the N/C ratio for the conventional NCNTs determined by XPS (0.0235) was lower than that determined by elemental analysis (0.0261), which was ascribed to the concentrated distribution of N atoms in the bamboo site inside the tube.[13] The electrical conductivity of the CNT@NCNT nanocables was determined as 3.3 S·cm^{-1} by the four-probe technique, over 3 times higher than that of the routine bamboo-like NCNTs, which was attributed to the undestroyed continuous inner walls in the CNT@NCNT.

With the integrated N atoms concentrated at the surface, the CNT@NCNT coaxial nanocables were expected to exhibit more effective 'active sites', consequently with better catalytic activity, than the bulk doped NCNTs with the similar doping level. Investigation of the electrocatalytic performance towards ORR and OER was performed as probe reactions to evaluate the catalytic property of the nanocarbon electrocatalysts. The doping content of nitrogen determined by XPS in the routine NCNTs is comparative with that in the CNT@NCNT nanocables. The specific surface areas of the three samples calculated by N_2 sorption isotherm were also comparative with each other (Table 1).

2.2. ORR Performance

The electrochemical measurement was carried out using a classical three-electrode electrochemical station with a saturated calomel electrode (SCE) and a platinum foil electrode as the reference and counter electrode, respectively. The electrocatalysts were supported on the glass carbon disk of a rotating ring-disk
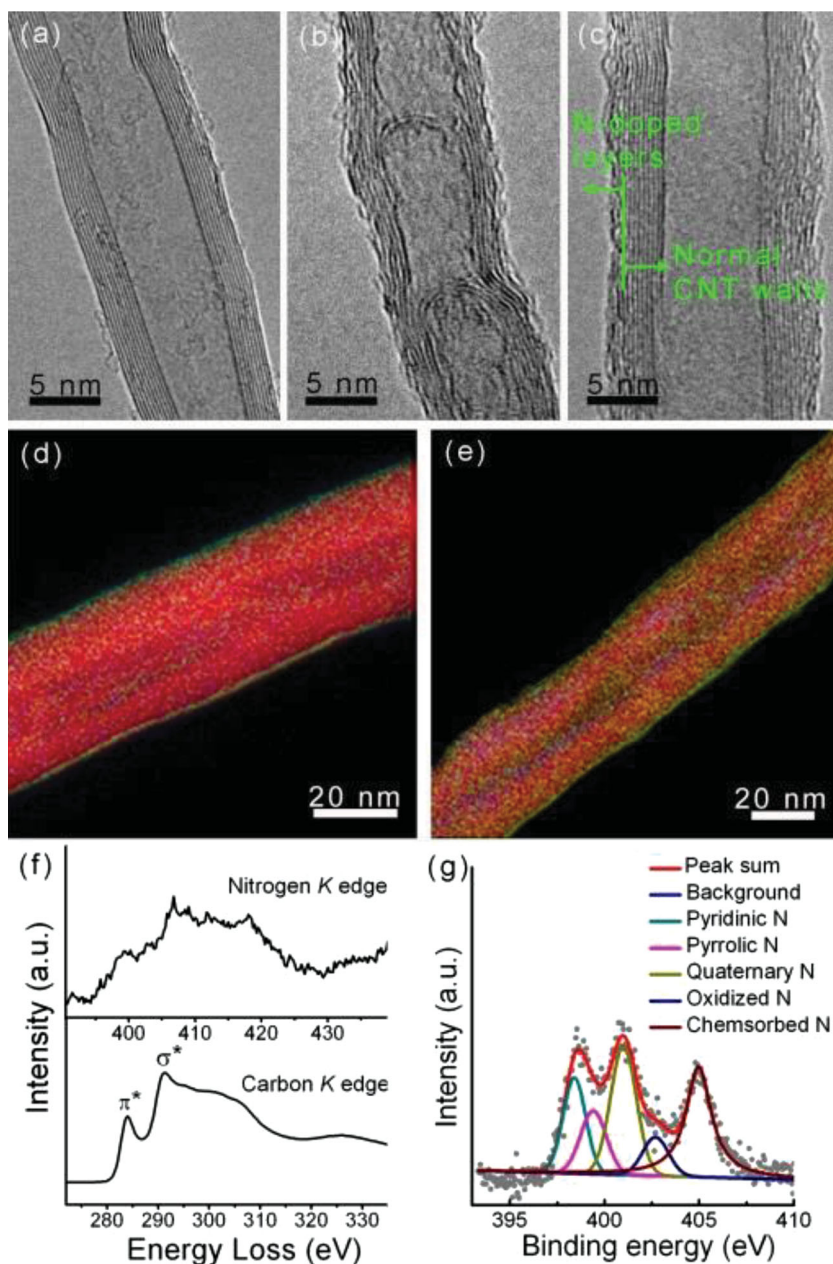

Figure 1. Scheme for the full exposure of 'active sites' on the surface: NCNTs with bulk doping of nitrogen atoms, while CNT@NCNT coaxial nanocables with surface enriched nitrogen for OER and ORR.

www.MaterialsViews.com

ADVANCED
FUNCTIONAL
MATERIALS
www.afm-journal.de

FULL PAPER

Figure 2. Structure of CNT@NCNT electrocatalyst with surface enriched nitrogen: TEM images of (a) pristine CNTs, (b) NCNTs, and (c) CNT@NCNT coaxial nanocables; the element mapping showing the distribution of N (green), C (red), and O (blue), of CNT@NCNT coaxial nanocables with the surface N/C ratio of (d) 0.0238 and (e) 0.0809; (f) high resolution EELS spectra of carbon K edge and nitrogen K edge and (g) N 1s core level XPS spectra for CNT@NCNT.

electrode (RRDE) as the working electrode. As shown in **Figure 3**a, the undoped pristine CNTs exhibited poor electrocatalytic activity for ORR with quite a negative onset potential −0.158 V and low cathodic current density compared with the NCNTs. The onset potential of CNT@NCNT nanocables was *ca.* −0.022 V, about 51 mV more positive than that of routine NCNTs. The disk current for the CNT@NCNT was higher than that for the NCNT catalyst, while the ring current ascribed to the generation of peroxide was much suppressed on the CNT@NCNT electrode. The peroxide yield, as well as the electron transfer number, calculated from the corresponding disk and ring current was illustrated in Figure 3b. The peroxide yield on the CNT@NCNT electrode is below 14.6% in a wide potential range from −0.2 to −0.8 V, indicating a four-electron pathway, whereas on the NCNT electrode the peroxide yield was averaged as high as ~30%. Accordingly, CNT@NCNT with surface enriched N atoms exhibited superior electrocatalytic activity for ORR in comparison with the bulk nitrogen doped CNTs. The durability evaluation of the CNT@NCNT electrocatalyst for ORR was also performed at the potential of −0.3 V with a rotating rate of 1600 rpm. As showed in Figure S6, a high relative current of 89.2% was still remained after 16000 s, indicating the high stability of the CNT@NCNT electrocatalyst. Furthermore, the optimized nanocable, CNT@NCNT-1 with an increased surface N/C ratio of 0.0809, a bulk N/C ratio 0.0472, and a *ca.* 1 nm thick N-doped carbon layer afford even better electrocatalytic performance with a more positive onset potential of −0.015 V, a peroxide yield below 8.68%, and the electron transfer number over 3.8 in the wide potential range from −0.2 to −0.8 V (Figure S7).

2.3. OER Performance

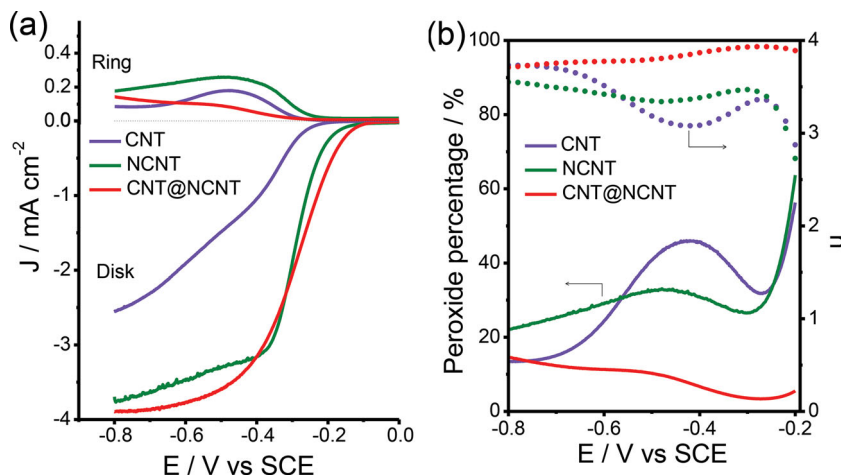When the potential applied on the working electrode was positively swept from 0 to 0.85 V with the scan rate of 5.0 mV s^{-1} and the

Table 1. Structure features of carbon electrocatalysts.

Sample	Surface N/C ratio[a]	Bulk N/C ratio[b]	SSA (m² g⁻¹)	I_D/I_G
CNT	−	−	211.0	1.32
NCNT	0.0235	0.0261	214.5	1.35
CNT@NCNT	0.0238	0.0219	208.0	1.34

[a]Determined by XPS analysis; [b]Determined by elemental analysis *via* combustion method.

Figure 3. (a) Rotating ring disk voltammograms recorded for CNT, NCNT, and CNT@NCNT electrode in an O_2-saturated 0.1 mol L^{-1} KOH solution at a scan rate of 5.0 mV s^{-1}. The disk current densities (bottom) and the corresponding ring current densities (top) are displayed separately as illustrated in the figure and the rotating speed of the electrode was 1600 rpm. (b) Percentage of peroxide (solid line) and the electron transfer number (n, dotted line) of the CNT, NCNT, and CNT@NCNT catalysts at various potentials, based on the corresponding RRDE data in (a).

rotating speed for the disk electrode was 1600 rpm, the OER catalytic activities were estimated in 0.1 mol L^{-1} KOH solution. The NCNTs displayed notably much improved OER current than the pristine CNTs (**Figure 4**a). CNT@NCNT nanocables exhibited higher OER catalytic activity with smaller overpotential than the routine NCNTs. The potential required for the current density of 10 mA cm^{-2} is an essential parameter relevant to solar fuel cells, which is widely used to evaluate the OER catalysts. As for the CNT@NCNT coaxial nanocables with the active sites concentrated on the surface, the potential corresponding to the current density of 10 mA cm^{-2} was ~0.75 V, about 20 mV more negative than that of the bulk doped NCNTs, suggesting a lower overpotential for OER. The polarization curves in Figure 4a were depicted into Tafel plots as presented in Figure 4b. At low overpotential, the OER mainly occurred under the electrochemical polarization. With the potential applied on the working electrode increasing, the oxygen evolution current on the electrode drift off the Tafel plot to a low current level due to the emerging concentration polarization caused by the slow and inefficient mass transfer at the interface between electrode and electrolyte. Compared with the NCNT, the concentration polarization emerged on the CNT@NCNT electrode at a relatively high overpotential, indicating more efficient and effective mass transfer on this electrode. The N atoms doping in CNT@NCNT were concentrated in the outer shell. Therefore, the active sites induced by the doping atoms are more accessible for the reactants as well as to improve the polarity and the hydrophily of the carbon material and hence facilitate the

mass transfer at the interface between electrode material and electrolyte.

2.4. The Relationship Between the Reactivity and Structure

To further assess the electrocatalytic activities of the NCNT and CNT@NCNT materials in comparison, the normalized current with respect to the incorporated N atoms and their turnover frequencies (TOFs) at different potentials in the ORR and OER regimes, respectively, were presented in **Table 2** and Figure S8. The TOFs of ORR were counted for the 4-electron process and the TOFs of the OER were calculated based on the hypothesis that the reaction occurred through a 4-electron pathway.[15] Take −0.50 V in ORR and 0.80 V in OER as examples, the current at the CNT@NCNT electrode normalized based on the N amount measured by elemental analysis (0.57 mA μgN^{-1} for ORR and 2.01 mA μgN^{-1} for OER) was much higher than that on the NCNT electrode (0.44 mA μgN^{-1} for ORR and 1.49 mA μgN^{-1} for OER), in spite of the less bulk N amount in CNT@NCNT nanocables. It was demonstrated that the dopant N atoms in the CNT@NCNT coaxial nanocables brought about more effective and efficient active sites for electrocatalysis. Moreover, the corresponding TOFs of the CNT@NCNT electrode were 0.112 and 0.421 s^{-1} for ORR and OER, respectively, in consistent with those of the Co based electrocatalysts[16] reported previously. The TOFs of the CNT@NCNT catalyst were higher than those of the NCNT catalyst in a wide potential range both for ORR and OER (Figure S8). The surface doped CNT@NCNT coaxial nanocables afforded effective
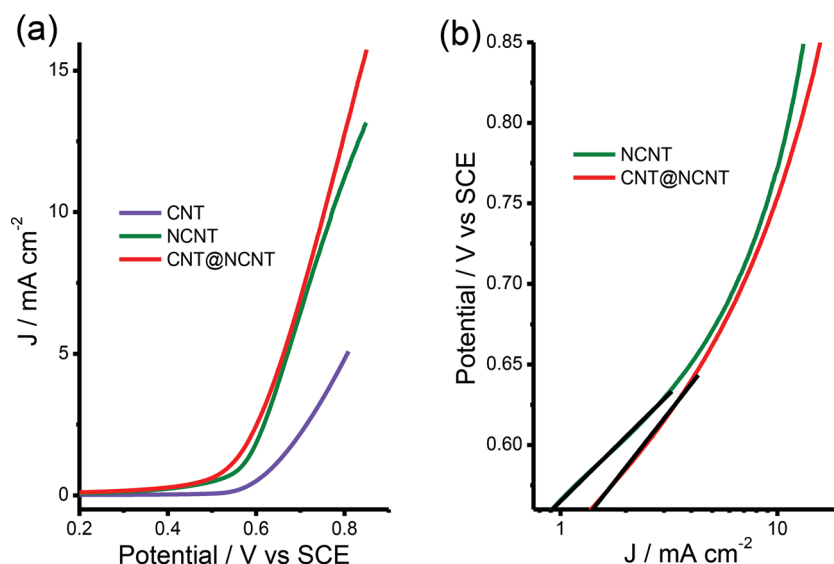

Figure 4. (a) OER currents of the CNT, NCNT, and CNT@NCNT catalysts in 0.1 mol L^{-1} KOH solution at a scan rate of 5.0 mV s^{-1}. (b) Tafel plots of OER currents for NCNT and CNT@NCNT in (a).

Table 2. The electrocatalysis performance on nanocarbon based electrocatalysts.

Sample	σ (S·cm^{-1})	J$_{ORR}$ (mA·µgN^{-1})[a]	J$_{OER}$ (mA·µgN^{-1})[a]	TOF (s^{-1})[b]	
				ORR	OER
NCNT	1.0	0.44	1.49	0.085	0.368
CNT@NCNT	3.3	0.57	2.01	0.112	0.421

[a]The potentials corresponding to the ORR current density and OER current density were −0.50 and 0.80 V vs SCE, respectively; [b]The TOFs of the ORR were counted for the 4-electron process and the TOFs of the OER were calculated based on the hypothesis that the reaction occurred in a 4-electron pathway.

exposure of 'active sites' at the surface and high conductive 3D scaffold. The low electrical resistance of CNT@NCNT facilitates the rapid charge transfer from the other NCNT layers into the CNT scaffolds. Consequently, superior electrocatalytic activities for both ORR and OER were available on the surface-exposed 'active sites', indicating that the novel CNT@NCNT nanocables can be a promising oxygen electrode material for URFCs.

3. Conclusions

We have reported the CNT@NCNT coaxial nanocables as a typical nanocarbon electrocatalyst with surface enriched nitrogen for superior oxygen reduction and evolution reactivity. The surface N/C ratios of the CNT@NCNT coaxial nanocables were easily modulated in the range from 0.0238 to 0.145 by changing the epitaxial growth duration. The CNT@NCNT coaxial nanocables afforded high electrical conductivity of 3.3 S cm^{-1}, much enhanced electrocatalytic activity towards ORR with ~51 mV positively shifted onset potential, low peroxide generation, and a preferential four-electron pathway. What's more, the as-obtained CNT@NCNT coaxial nanocables also exhibited superior electrocatalytic activity for OER with higher oxygen evolution current in comparison with the routine bulk dope NCNTs under the same conditions. The accessible and efficient utilization of the integrated N atoms enriched on the surface, combined with the intact undestroyed inner walls, rendered the CNT@NCNT coaxial nanocables as a promising bifunctional electrocatalyst for ORR and OER. Besides, the CNT@NCNT coaxial nanocables were good platform towards full exposure of 'active sites' for robust interfaces for high performance composites, as well as efficient catalysts and/or metal nanoparticle supports for selective oxidation of alkane, biosensors, etc. Since the surface hetero-junction nanostructures are not limited to CNTs, we foresee a new branch of chemistry evolving in the area of full exposure of active sites through the 3D heterogeneous systems.

4. Experimental Section

4.1. Synthesis of Nanocarbon Electrocatalyst with Surface Enriched Nitrogen

The CNT@NCNT electrocatalysts were prepared with simple chemical vapor deposition (CVD) of nitrogen containing pyrolytic carbon on the surface of pure CNTs. The CNTs were mass produced on Fe catalysts in the fluidized bed reactor and purified by high temperature annealing. The catalyst was removed by routine acid treatment and high-vacuum

annealing for very high purity CNTs. 300 mg CNTs were distributed uniformly on a quartz boat which was then placed at the center of a horizontal quartz tube. The quartz tube reactor was then inserted into a tube furnace which was heated to 760 °C at atmosphere pressure under flowing Ar (200 mL min^{-1}). The pyridine with a flow rate of 1.5 mL h^{-1} was fed into the reactor using a syringe pump. The deposition of doped carbon was maintained for an anticipated duration before the furnace was cooled down to room temperature under Ar protection. The conversion of pyridine into the wrinkled N-doped layers was estimated to be ca. 10.1%. The as-obtained nitrogen doped CNT products were denoted as CNT@NCNT coaxial nanocables.

4.2. Structural Characterizations

The morphology and structure of the as-produced CNT@NCNT coaxial nanocables were characterized using a JSM 7401F scanning electron microscope (SEM) operated at 3.0 kV and a JEM 2010 high-resolution transmission electron microscope (HRTEM) operated at 120.0 kV. The energy filtered transmission electron microscope (EFTEM) images of the CNT@NCNT products were collected on a FEI Tecnai G^2 F20 TEM equipped with Gatan Image Filter (GIF) to detect the distribution of C, N, and O element in one CNT@NCNT coaxial nanocable. X-ray photoelectron spectroscopy (XPS) operated by Escalab 250xi was employed to determine the amount of nitrogen-containing functional groups in the samples. Raman spectra were collected with He-Ne laser excitation at 633 nm using Horiba Jobin Yvon LabRAM HR800 Raman spectrophotometer. The Brunauer–Emmett–Teller (BET) SSA of the samples were measured by N$_2$ adsorption/desorption at liquid-N$_2$ temperature using Autosorb-IQ2-MP-C system. The elemental analysis was performed on an Elemental Analyzer (Elementar Americas/Model: Vario EL III). The electrical conductivity of the NCNT and CNT@NCNT was measured using the KDY-1 four-probe technique.

4.3. Electrocatalytic Performance Measurements

The as-synthesized CNT@NCNT samples, together with the pristine CNTs and the conventional bulk doped NCNTs, were firstly dispersed in ethanol (5.0 mg mL^{-1}) by sonication. 10 µL CNT or N-doped CNT suspension was pipetted onto the glass carbon disk electrode surface, which was polished mechanically with 0.05 µm alumina slurry and then washed with deionized water and acetone to obtain a mirror-like clean surface prior to use. After solvent evaporation for 10 min in air, a thin layer of Nafion solution (1 wt%) was coated onto the electrode surface and then dried in an oven at 60 °C for 30 min before measurement.

The electrochemical measurements were conducted on an RRDE configuration (Pine Research Instrument, USA) in a three-electrode electrochemical cell using a computer-controlled potentialstation (CHI 760D, CH Instrument, USA). A rotating ring disk electrode with a disk diameter of 5 mm served as the substrate for the working electrode. A saturated calomel electrode (SCE) and Pt foil electrode were used as the reference and counter electrode, respectively. The OER activities of all the samples were evaluated by the linear sweep voltammetry method with a potential range scanned from 0.2 to 0.85 V versus SCE at the scan rate of 5.0 mV s^{-1} in O$_2$-saturated 0.1 mol L^{-1} KOH solution. During

FULL PAPER

the tests, the disk electrode was rotating at a speed of 1600 rpm. The oxygen reduction tests were carried out in O_2-saturated 0.1 mol L^{-1} KOH solution at room temperature. The disk electrode was scanned cathodically at a rate of 5.0 mV s^{-1} in the potential range of 0.2 to −0.8 V versus SCE and the ring potential was set constant at +0.5 V versus SCE to monitor the formation of peroxide intermediate. The electron transfer number n and HO_2^- intermediate production percentage (%HO_2^-) were calculated based on the disk and ring current as followed:

$$n = \frac{4I_d}{I_d + I_r/N} \tag{1}$$

$$\%HO_2^- = \frac{200I_d/N}{I_d + I_r/N} \tag{2}$$

where I_d is disk current, I_r is ring current and N is current collection efficiency of the Pt ring which was determined to be 0.26.

Supporting Information

Supporting Information is available from the Wiley Online Library or from the author.

Acknowledgements

[1] a) J. Suntivich, K. J. May, H. A. Gasteiger, J. B. Goodenough, Y. Shao-Horn, *Science* **2011**, *334*, 1383; b) D. W. Wang, D. S. Su, *Energy Environ. Sci.* **2014**, *7*, 576; c) H. Dau, C. Limberg, T. Reier, M. Risch, S. Roggan, P. Strasser, *ChemCatChem* **2010**, *2*, 724; d) U. N. Maiti, W. J. Lee, J. M. Lee, Y. Oh, J. Y. Kim, J. E. Kim, J. Shim, T. H. Han, S. O. Kim, *Adv. Mater.* **2014**, *26*, 40; e) S. J. Guo, S. Zhang, S. H. Sun, *Angew. Chem. Int. Ed.* **2013**, *52*, 8526; f) K. S. Joya, Y. F. Joya, K. Ocakoglu, R. van de Krol, *Angew. Chem. Int. Ed.* **2013**, *52*, 10426; g) I. Katsounaros, S. Cherevko, A. R. Zeradjanin, K. J. J. Mayrhofer, *Angew. Chem. Int. Ed.* **2014**, *53*, 102.

[2] S. Park, Y. Y. Shao, J. Liu, Y. Wang, *Energy Environ. Sci.* **2012**, *5*, 9331.

[3] a) T. Reier, M. Oezaslan, P. Strasser, *ACS Catal.* **2012**, *2*, 1765; b) Y. Y. Liang, H. L. Wang, P. Diao, W. Chang, G. S. Hong, Y. G. Li, M. Gong, L. M. Xie, J. G. Zhou, J. Wang, T. Z. Regier, F. Wei, H. J. Dai, *J. Am. Chem. Soc.* **2012**, *134*, 15849.

[4] a) Q. Liu, J. T. Jin, J. Y. Zhang, *ACS Appl. Mater. Interfaces* **2013**, *5*, 5002; b) Y. Gorlin, T. F. Jaramillo, *J. Am. Chem. Soc.* **2010**, *132*, 13612; c) Y. Y. Liang, Y. G. Li, H. L. Wang, J. G. Zhou, J. Wang, T. Regier, H. J. Dai, *Nat. Mater.* **2011**, *10*, 780; d) Y. G. Li, W. Zhou, H. L. Wang, L. M. Xie, Y. Y. Liang, F. Wei, J. C. Idrobo, S. J. Pennycook, H. J. Dai, *Nat. Nanotechnol.* **2012**, *7*, 394; e) Y. Zheng, Y. Jiao, L. Ge, M. Jaroniec, S. Z. Qiao, *Angew. Chem. Int. Ed.* **2013**, *52*, 3110; f) Y. Jiao, Y. Zheng, M. Jaroniec, S. Z. Qiao, *J. Am. Chem. Soc.* **2014**, *136*, 4394.

[5] a) Y. Zhao, R. Nakamura, K. Kamiya, S. Nakanishi, K. Hashimoto, *Nat. Comm.* **2013**, *4*, 2390; b) D. S. Yu, K. L. Goh, L. Wei, H. Wang, Q. Zhang, W. C. Jiang, R. M. Si, Y. Chen, *J. Mater. Chem. A* **2013**, *1*, 11061; c) S. Y. Wang, E. Iyyamperumal, A. Roy, Y. H. Xue, D. S. Yu, L. M. Dai, *Angew. Chem. Int. Ed.* **2011**, *50*, 11756; d) S. Chen, J. Y. Bi, Y. Zhao, L. J. Yang, C. Zhang, Y. W. Ma, Q. Wu, X. Z. Wang, Z. Hu, *Adv. Mater.* **2012**, *24*, 5593; e) Z. W. Liu, F. Peng, H. J. Wang, H. Yu, W. X. Zheng, J. A. Yang, *Angew. Chem. Int. Ed.* **2011**, *50*, 3257; f) H. Yu, F. Peng, J. Tan, X. W. Hu, H. J. Wang, J. A. Yang, W. X. Zheng, *Angew. Chem. Int. Ed.* **2011**, *50*, 3978; g) Q. Q. Li, S. Zhang, L. M. Dai, L. S. Li, *J. Am. Chem. Soc.* **2012**, *134*, 18932; h) Y. Li, Y. Zhao, H. H. Cheng, Y. Hu, G. Q. Shi, L. M. Dai, L. T. Qu, *J. Am. Chem. Soc.* **2012**, *134*, 15; i) H. Zhu, J. Yin, X. L. Wang, H. Y. Wang, X. R. Yang, *Adv. Funct. Mater.* **2013**, *23*, 1305; j) D. S. Yu, L. Wei, W. Jiang, H. Wang, B. Sun, Q. Zhang, K. Goh, R. Si, Y. Chen, *Nanoscale* **2013**, *5*, 3457; k) W. Wei, H. W. Liang, K. Parvez, X. D. Zhuang, X. L. Feng, K. Mullen, *Angew. Chem. Int. Ed.* **2014**, *53*, 1570; l) S. Chen, J. Duan, M. Jaroniec, S.-Z. Qiao, *Adv. Mater.* **2014**, *26*, 2925.

[6] K. P. Gong, F. Du, Z. H. Xia, M. Durstock, L. M. Dai, *Science* **2009**, *323*, 760.

[7] a) S. B. Yang, L. J. Zhi, K. Tang, X. L. Feng, J. Maier, K. Mullen, *Adv. Funct. Mater.* **2012**, *22*, 3634; b) R. L. Liu, D. Q. Wu, X. L. Feng, K. Mullen, *Angew. Chem. Int. Ed.* **2010**, *49*, 2565; c) D. S. Yu, Q. Zhang, L. M. Dai, *J. Am. Chem. Soc.* **2010**, *132*, 15127; d) G. L. Tian, M. Q. Zhao, D. S. Yu, X. Y. Kong, J. Q. Huang, Q. Zhang, F. Wei, *Small* **2014**, *10*, 2251; e) D. H. Deng, L. Yu, X. Q. Chen, G. X. Wang, L. Jin, X. L. Pan, J. Deng, G. Q. Sun, X. H. Bao, *Angew. Chem. Int. Ed.* **2013**, *52*, 371.

[8] R. J. Nicholls, A. T. Murdock, J. Tsang, J. Britton, T. J. Pennycook, A. Koos, P. D. Nellist, N. Grobert, J. R. Yates, *ACS Nano* **2013**, *7*, 7145.

[9] a) J. Liang, X. Du, C. Gibson, X. W. Du, S. Z. Qiao, *Adv. Mater.* **2013**, *25*, 6226; b) S. Chen, J. J. Duan, M. Jaroniec, S. Z. Qiao, *Angew. Chem. Int. Ed.* **2013**, *52*, 13567; c) M. Sevilla, L. Yu, L. Zhao, C. O. Ania, M.-M. Titiricic, *ACS Sustainable Chem. Eng.* **2014**, *2*, 1049; d) Y. J. Sa, C. Park, H. Y. Jeong, S.-H. Park, Z. Lee, K. T. Kim, G.-G. Park, S. H. Joo, *Angew. Chem. Int. Ed.* **2014**, *53*, 4102; e) D. S. Su, S. Perathoner, G. Centi, *Chem. Rev.* **2013**, *113*, 5782.

[10] a) G. L. Tian, M. Q. Zhao, Q. Zhang, J. Q. Huang, F. Wei, *Carbon* **2012**, *50*, 5323; b) G. K. Goswami, R. Nandan, K. K. Nanda, *Carbon* **2013**, *56*, 97; c) H. B. Li, W. J. Kang, L. Wang, Q. L. Yue, S. L. Xu, H. S. Wang, J. F. Liu, *Carbon* **2013**, *54*, 249; d) Y. X. Wang, X. Z. Cui, Y. S. Li, L. S. Chen, H. R. Chen, L. X. Zhang, J. L. Shi, *Carbon* **2014**, *68*, 232; e) Z. Y. Mo, S. J. Liao, Y. Y. Zheng, Z. Y. Fu, *Carbon* **2012**, *50*, 2620.

[11] J. Q. Huang, M. Q. Zhao, Q. Zhang, J. Q. Nie, L. D. Yao, D. S. Su, F. Wei, *Catal. Today* **2012**, *186*, 83.

[12] Q. Zhang, J. Q. Huang, W. Z. Qian, Y. Y. Zhang, F. Wei, *Small* **2013**, *9*, 1237.

[13] I. Florea, O. Ersen, R. Arenal, D. Ihiawakrim, C. Messaoudi, K. Chizari, I. Janowska, J. Pham-Huu, *J. Am. Chem. Soc.* **2012**, *134*, 9672.

[14] a) J. Zhang, D. S. Su, A. H. Zhang, D. Wang, R. Schlogl, C. Hebert, *Angew. Chem. Int. Ed.* **2007**, *46*, 7319; b) C. L. Chen, J. Zhang, B. S. Zhang, C. L. Yu, F. Peng, D. S. Su, *Chem. Commun.* **2013**, *49*, 8151.

[15] M. Gong, Y. G. Li, H. L. Wang, Y. Y. Liang, J. Z. Wu, J. G. Zhou, J. Wang, T. Regier, F. Wei, H. J. Dai, *J. Am. Chem. Soc.* **2013**, *135*, 8452.

[16] a) B. S. Yeo, A. T. Bell, *J. Am. Chem. Soc.* **2011**, *133*, 5587; b) X. Zou, A. Goswami, T. Asefa, *J. Am. Chem. Soc.* **2013**, *135*, 17242.